Study on Retrieving Three-Dimensional Wind Using Simulated Dual-Doppler Radar Data in the Cartesian Space*

ZHOU Haiguang (周海光) and ZHANG Peiyuan (张沛源)

State Key Laboratory of Severe Weather, Chinese Academy of Meteorological Sciences, Beijing 100081

(Received May 30, 2005)

ABSTRACT

This paper investigates a technique of retrieving three-dimensional wind fields from the dual-Doppler weather radar radial wind which is based on the Cartesian space using variational method. This technology provides a simultaneous resolution of three wind components and satisfies both the minimal dual-equation system and the continuity equation. The main advantage of this method is that it can remove the potential drawback of an iterative solution of Cartesian dual-Doppler analysis techniques which is a major demerit when one retrieves the vertical velocity using mass continuity equation with iterative method. The data pre-processing technology and interpolation are also studied. This work developed a three-dimensional Cressman weighting function to process the interpolation. In order to test the capability and advantage of this method, one numerical experiment based on simulating dual-Doppler radar observations is designed. Firstly, we synthesize the dual-Doppler radar radial velocity and reflectivity from the numerical model. Then, the three-dimensional wind components are retrieved from the radial velocity and reflectivity using this technique. The retrieved three-dimensional wind fields are found to be quite consisted with those previously simulated wind fields. Mean difference, root-mean-square error, and relative deviation are defined to test the precision of the method. These statistic errors reveal the accuracy and the advantage of this method. The numerical experiment has definitely testified that this technique can be used to retrieve the three-dimensional wind fields from the radial velocity and reflectivity detected by the real dual-Doppler weather radar.

Key words: dual-Doppler weather radar, three-dimensional wind fields, variational method, interpolation, retrieval

1. Introduction

Armijo (1969) proposed the three-dimensional wind retrieved equations using multiple-Doppler weather radar network in Cartesian space. There are many sources of error for recovering 3D wind using these equations. These factors include advection and turbulence in the weather system, the error of the empirical relationship between the radar reflectivity factor and the terminal fall velocity of the precipitation particle, integrating the air mass continuity equation (problem of the boundary condition), the non-simultaneous nature of the data acquisition (due to the temporal variation within the volume scan time interval), spatial interpolation, and filter errors. All of these problems have not been solved till now.

To evaluate these problems in some degree, Lhermitte and Miller (1970) proposed the COPLANE dual-Doppler radar observation methodology which improved by Miller and Strauch (1974) later. Ray et al. (1980) proposed overdetermined dual-Doppler (ODD) method to retrieve wind filed using Euler equation. Chong and Campos (1996) proposed an extended ODD (EODD) technique to solve the iterative problem. Bousquet and Chong (1998) proposed the multiple-Doppler synthesis and continuity adjustment technique (MUSCAT) in retrieved 3D wind from airborne Doppler radars which deduced the 3D wind in one step using variational method.

In 2001, under the support of the National Key Basic Research and Development Project "Research on the Formation Mechanism and the Prediction Theory of Hazardous Weather over China", we installed two dual-Doppler radar networks to study the severe

*This work is supported by the National Key Basic Research and Development Project of China (2004CB418305), by the National Natural Science Foundation of China under Grant No. 40375006, and by the project of Ministry of Science and Technology of China (2002DIA20013).

weather in the field experiment. It also started the dual-Doppler radar wind retrieval technique in mainland of China. This paper studied the dual-Doppler radar three-dimensional wind retrieval technology. In order to improve the result reasonability and retrieval accuracy, some new methods were also proposed including raw radar data pre-processing, spatial interpolation, and result evaluation.

2. Retrieval technology

2.1 *Coordinate system*

The following Cartesian coordinate system is designed for the purpose of retrieval. The first radar was located at the origin, x axis is directed to east, y axis is directed to north, and z axis points in the direction opposite to the gravity vector.

In all the former retrieved techniques, the earth's curvature is ignored. It makes the retrieval difficult because the microwave transmission curve is not straight and the earth's surface is not flat (Zhang et al., 2002). In order to reveal the wind structure with better accuracy, this problem must be solved. The earth can be treated as a sphere in a small area. Based on this assumption, the coordinate transforms from a radar polar coordinate system to a Cartesian coordinate system are defined as follows

$$\begin{cases} x = R\cos[\theta + \beta(\phi)]\sin(\phi - \alpha) \\ y = R\cos[\theta + \beta(\phi)]\cos(\phi - \alpha), \\ z = R\sin[\theta + \beta(\phi)] \end{cases} \tag{1}$$

where x, y, and z are the coordinate in the Cartesian space. R, θ, and Φ are the slant range, elevation angle, and azimuth angle respectively in the radar polar coordinate system. $\beta(\phi)$ denotes the elevation angle correct function. It is related to the Φ as follows

$$\beta(\phi) = \left[\arctan\left(\frac{L}{R_o}\right)\right](\phi - \alpha)/90 \qquad 0^\circ \leqslant \phi - \alpha < 90^\circ$$

$$\beta(\phi) = \left[\arctan\left(\frac{L}{R_o}\right)\right][180 - (\phi - \alpha)]/90 \qquad 90^\circ \leqslant \phi - \alpha < 180^\circ$$

$$\beta(\phi) = -\left[\arctan\left(\frac{L}{R_o}\right)\right][(\phi - \alpha) - 180]/90 \qquad 180^\circ \leqslant \phi - \alpha < 270^\circ$$

$$\beta(\phi) = -\left[\arctan\left(\frac{L}{R_o}\right)\right][360 - (\phi - \alpha)]/90 \qquad 270^\circ \leqslant \phi - \alpha < 360^\circ, \tag{2}$$

where α is the angle between y direction and north, L is the radar base line, and R_o is the equivalent earth's radius (8500 km).

2.2 *Raw radar data interpolation method*

Now the dual-Doppler radar works in the volume scan strategy. Thus, all the raw data observed by the two radars must be interpolated to the grid points in the Cartesian coordinate system from the radar polar coordinate system before retrieving.

There are many methods to interpolate the raw radar data. The two-dimensional Cressman distance-weighted interpolation was often used (Cressman, 1959) in dual-Doppler radar analysis. In this paper, a three-dimensional Cressman distance-weight interpolation function was adopted because the interpolation was done in the three-dimensional Cartesian coordinate system. We define the following function

$$F = \frac{\sum \omega_i f_i}{\sum \omega_i}, \tag{3}$$

where f_i denotes the ith observation value by radar, ω_i is the Cressman distance-weighted coefficient depending on the distance between the ith observation point and the grid point. It is defined as

$$\omega_i = \begin{cases} \dfrac{R_i^2 - D_i^2}{R_i^2 + D_i^2} & D_i \leqslant R_i \\ 0 & D_i > R_i, \end{cases} \tag{4}$$

where D_i is the distance between the ith observation point and the grid point. R_i is the influence radius defined as

$$R_i = \frac{R_H R_z}{(R_H^2 \sin^2 \Psi_i + R_z^2 \cos^2 \Psi_i)^{\frac{1}{2}}} \tag{5}$$

$$\Psi_i = \arctan\left[\frac{z_i}{(x_i^2 + y_i^2)^{\frac{1}{2}}}\right] \tag{6}$$

where R_H and R_z are the horizontal and vertical influence radius, respectively. x_i, y_i, and z_i denote the observation point's coordinate relative to the grid point in the Cartesian space. Ψ_i denotes the elevation angle

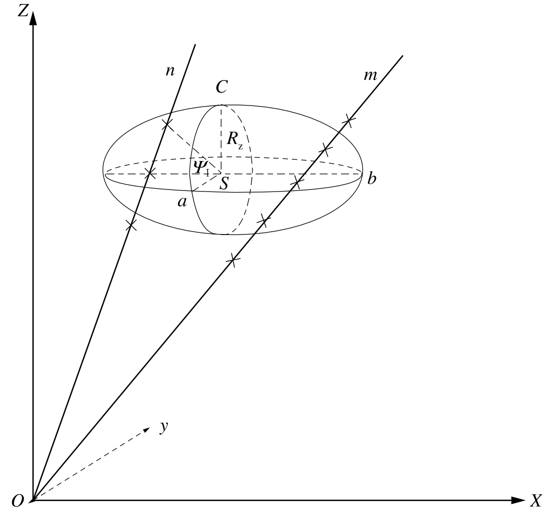

Fig.1. Data interpolation.

of the observation point relative to the grid point.

Figure 1 gives the Cressman interpolation function legend. Wherefrom s (center of the ellipsoid) denotes the grid point. sa and sc denote the horizontal semi-axis radius (horizontal influence radius) and vertical semi-axis radius (vertical influence radius) of the ellipsoid, respectively. Radar is located in the origin of the coordinate system. om and on define the two scan lines of the radar. The asterisk on the scan line defines the radar's observation point. The value at grid point s can be obtained from the radar observation points which fall inside the ellipsoid using the Cressman distance-weighted function.

2.3 *Wind retrieval technology*

The MUSCAT proposed by Bousquet and Chong (1998) is commonly used in retrieving 3D wind field from the airborne Doppler radars. In this paper, we developed this method to retrieve the ground-based dual-Doppler radar 3D wind.

Based on the variational method MUSCAT defines the following functional F

$$F = \int_S [A(u,v,w)+B(u,v,w)+C(u,v,w)]\mathrm{d}x\mathrm{d}y. \tag{7}$$

Solution for the velocity field (u, v, w) is retrieved according to a simultaneous resolution of

$$\frac{\partial F}{\partial u} = 0,\ \frac{\partial F}{\partial v} = 0,\ \frac{\partial F}{\partial w} = 0, \tag{8}$$

and the flexible boundary condition is used when solving the equations. In Eq.(7) terms A, B, and C are expressions that represent the least squares fit of observed radial velocities to wind components, the least squares adjustment of continuity equation, and the filtering of small-scale variations of the wind components, respectively.

The data fit term A is defined as

$$A_{ij} = \frac{1}{N}\sum_{p=1}^{n_p}\sum_{q=1}^{n_q(p)} \omega_q[\alpha_q u + \beta_q v + \gamma_q(w + W_t) - V_q]^2, \tag{9}$$

$$\alpha_q = \sin\theta_q \cos\alpha_q, \tag{10}$$

$$\beta_q = \cos\theta_q \cos\alpha_q, \tag{11}$$

$$\gamma_q = \sin\alpha_q, \tag{12}$$

where u, v, and w indicate velocities at the grid point, respectively. W_t is the terminal fall velocity of precipitation particles for the grid point. ω_q is the Cressman weighting function which can be obtained from Eq.(4). V_q is the radial velocity. Subscript q means the qth measurement of a total number n_q which falls inside an ellipsoid of influence centered at the point. P defines the number of radars ($p \geqslant 2$). θ_q and α_q denote azimuth angle (clockwise direction from the north) and elevation angle, respectively.

The adjustment term B is defined as

$$B = \mu_1\left(\frac{\partial u}{\partial x} + \frac{\partial v}{\partial y} + \frac{1}{\rho}\frac{\partial \rho w}{\partial z}\right)^2. \tag{13}$$

Because the air density is a variable of the three-dimensional atmosphere, it can be rewritten as

$$B = \mu_1\left[\frac{\partial \rho u}{\partial x} + \frac{\partial \rho v}{\partial y} + \frac{\partial \rho w}{\partial z}\right]^2. \tag{14}$$

Equation (14) is more reasonable and can improve the retrieval accuracy.

Filter term C is defined as

$$C = \mu_2\Big[J(u) + J'(u) + J(v) + J'(v) + J(w) + J'(w)\Big], \tag{15}$$

$$J = \left(\frac{\partial^2}{\partial x^2}\right)^2 + 2\left(\frac{\partial^2}{\partial x \partial y}\right)^2 + \left(\frac{\partial^2}{\partial y^2}\right)^2, \tag{16}$$

$$J'(u) = \mu_1\left[\left(\frac{\partial^3 u}{\partial x^3}\right)^2 + 2\left(\frac{\partial^3 u}{\partial x^2 \partial y}\right)^2 + \left(\frac{\partial^3 u}{\partial x \partial y^2}\right)^2\right], \tag{17}$$

$$J'(v) = \mu_1\left[\left(\frac{\partial^3 v}{\partial y^3}\right)^2 + 2\left(\frac{\partial^3 v}{\partial x \partial y^2}\right)^2 + \left(\frac{\partial^3 v}{\partial x^2 \partial y}\right)^2\right], \tag{18}$$

$$J'(w) = \mu_1\left[\left(\frac{\partial^3 w}{\partial x^2 \partial z}\right)^2 + \left(\frac{\partial^3 w}{\partial y^2 \partial z}\right)^2 + 2\left(\frac{\partial^3 w}{\partial x \partial y \partial z}\right)^2\right], \tag{19}$$

where μ_1 and μ_2 are weighting parameters that can be found in the paper by Bousquet and Chong (1998).

3. Simulation experiment

A simulation experiment was designed in order to evaluate the performance of this retrieval method. Firstly, the simulated dual-Doppler radar radial velocity and reflectivity were deduced from the 3D wind field and water content of clouds given by a three-dimensional cloud numerical model. Secondly, the three-dimensional wind fields were retrieved from the simulated radial velocity and reflectivity. Finally, the retrieved wind fields were compared with the numerical model's winds in order to evaluate the accuracy of the retrieval.

3.1 *Simulation data*

The simulated 3D wind field, temperature, and water content of clouds were calculated by a three-dimensional numerical cloud model (Xu and Wei, 1995). The model comprises 40×40×25 grid points. The grid interval is 1 km in the horizontal and 0.5 km in the vertical. Figure 2 is the coordinate system of dual-Doppler radar in which the earth curvature is assumed. The radar baseline is 80 km. The line along the radar baseline is x axis and y axis is directed to north. The west radar is located at the origin of coordinate and the east radar is located at point (80, 0, 0). The simulated space is located on the north of the baseline. ABCD denotes the rectangle at the earth's surface. The four points are located at (20, 20, 0), (60, 20, 0), (60, 60, 0), and (20, 60, 0), respectively. h denotes the radar antenna altitude, (x, y, H) denotes the coordinate of point E in the Cartesian space. r, θ, and φ denote the slant range, elevation angle, and azimuth angle, respectively.

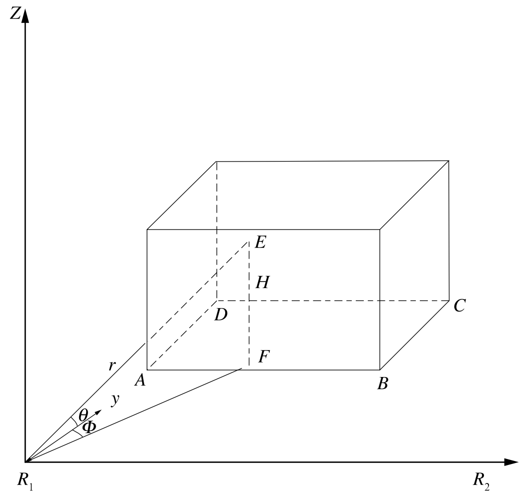

Fig.2. Dual-Doppler radar coordinate system when the earth's curvature is assumed.

When the earth's curvature and the earth's atmosphere refraction are assumed, the coordinate transform expression for the first radar is written as

$$H = h + r\sin\theta + \frac{r^2}{17008}, \tag{20}$$

$$r = \left[x^2 + y^2 + H^2\right]^{\frac{1}{2}}, \tag{21}$$

$$\theta = \arctan\left(\frac{x}{y}\right). \tag{22}$$

The coordinate transform expression for the second radar is written as

$$H = h + r\sin\theta + \frac{r^2}{17008}, \tag{23}$$

$$r = \left[(x-80)^2 + y^2 + H^2\right]^{\frac{1}{2}}, \tag{24}$$

$$\theta = \arctan\left(\frac{x-80}{y}\right). \tag{25}$$

The air density and the temperature has the following relationship (Doviak and Dusan, 1984)

$$\rho = \rho_0 \exp\left(\frac{-gNr\sin\theta}{RT}\right), \tag{26}$$

where ρ_0 denotes the air density at the earth's surface, g is the gravitational constant, N is the mean molecular weight of air, r is the slant range, θ is the elevation angle, R is the universal gas constant, and T is the absolute temperature.

The relationship between reflectivity factor (Z) and water content of clouds (M) can be written as

$$Z = 3.8 \times 10^2 \times M^{1.46}. \tag{27}$$

The terminal velocity (W_t) of precipitation particles and the reflectivity factor (Z) have the following form

$$W_t = 2.65Z^{0.114}(\frac{\rho_0}{\rho})^{0.4} \tag{28}$$

Then, the terminal velocity of precipitation particles can be obtained from temperature and water content of clouds based on Eqs.(26)-(28).

According to the radar observation strategy, the radar volume scan includes 16 layers with the elevation angles being 0°, 0.5°, 1.0°, 1.5°, 2.0°, 2.5°, 3.0°, 4.0°, 5.0°, 6.0°, 8.0°, 10.0°, 12.0°, 15.0°, 18.0°, and 21.0°, respectively. The azimuth angle interval is 1°. The radial gate is 300 m. The coordinate transform from radar polar coordinate system to Cartesian coordinate system is deduced from Eq.(1). Because the radar detecting point and the grid point of the 3D numerical model are not coincident in the Cartesian space, the value at the radar detecting point was interpolated by all the data contained within an ellipsoid volume using Cressman function.

The radar radial velocity can be formulated as

$$\begin{aligned} V_r(x,y,z) = \frac{1}{R_1}[(x-x_1)u + (y-y_1)v \\ +(z-z_1)(w+W_t)], \end{aligned} \tag{29}$$

where $R_1 = [(x-x_1)^2 + (y-y_1)^2(z-z_1)^2]^{\frac{1}{2}}$, ($x$, y, z) describes the radar's location, and (x_1, y_1, z_1) denotes the observation point.

The reflectivity at the observation point is deduced from Eq.(27).

3.2 *Procedure of the simulation experiment*

Zhang et al. (1998) have studied the optimum locations of three radars in retrieving wind. They proposed that if radar's measuring velocity precision is 1 m s^{-1}, the optimum distance of radars is 0.55 L, where L is the radar maximum detection range. Based on this result, the radar baseline is taken as 80 km in our paper.

The radial velocities observed by the two simulated radars can be obtained from equations in Section 3.1. Finally, the 3D wind field can be obtained from Eq.(8).

To measure the retrieval accuracy, we calculated the following error statistics.

Mean difference is given by

$$M_u = \frac{\sum_{i=1}^{N}(U_{\mathrm{r}i} - U_{\mathrm{o}i})}{N}, \tag{30}$$

root mean square is given by

$$\sigma_u = \sqrt{\frac{\sum_{i=1}^{N}(U_{\mathrm{r}i} - U_{\mathrm{o}i})^2}{N}}, \tag{31}$$

relative deviation is taken as

$$d_u = \frac{\sum_{i=1}^{N}(U_{\mathrm{r}i} - U_{\mathrm{o}i})}{\sum_{i=1}^{N}U_{\mathrm{o}i}} \times 100\%, \tag{32}$$

where the subscript "r" denotes the retrieved velocity. The subscript "o" denotes the simulated velocities given by numerical modeling. N is the total number of grid points. The proportions of the relative deviation less than 5%, 10%, 15%, and 20% are also calculated.

3.3 *Analysis of results*

3.3.1 *Error statistics analysis*

The error statistics of u, v, and w are listed in Tables 1, 2, and 3, respectively. The error statistics at the first level are not calculated because it is the earth's surface. M_u and σ_u below the 8 km level are smaller. d_u less than 15% accounts for more than 70% of cases below 8 km level. It means that the retrieval is quite good. The error statistics of v are very similar. The result at higher levels is worse than that at lower levels. M_w and σ_w increase with altitude. In comparison, the accuracy at low altitudes is superior to that at high levels. In general, the retrieved result below 8 km is quite reasonable. It is shown that MUSCAT has a real ability to retrieve the 3D wind field.

3.3.2 *Velocity analysis*

Figures 3, 4, and 5 show the simulated wind field and retrieved wind field at 3, 5, and 7 km levels, respectively.

Figure 3 compares the simulated and retrieved velocity at 3 km altitude. As can be seen in the figures, the retrieved wind filed exhibits a high degree of similarity to the simulated wind field. The position of the storm center retrieved from MUSCAT is quite similar to the simulated one. The pattern of the vertical velocity retrieved from MUSCAT is also analogous to the simulated one.

Table 1. Error statistics of u at different height

Height (km)	Mean difference	Root mean square	Proportion on relative deviation			
			<5%	<10%	<15%	<20%
0.5	-1.23	1.28	98.36	98.88	99.22	99.39
1.0	-0.63	0.79	95.42	96.11	96.54	97.06
1.5	-0.14	0.65	91.87	92.82	93.43	94.03
2.0	0.12	0.79	72.75	85.03	91.70	92.56
2.5	0.29	0.92	65.59	67.25	74.48	82.01
3.0	0.42	0.97	61.31	62.73	64.46	73.46
3.5	0.42	0.93	66.90	62.55	71.92	75.55
4.0	0.30	0.85	83.74	85.03	85.90	86.76
4.5	0.37	0.85	95.33	96.71	97.06	97.32
5.0	0.30	0.83	93.69	95.33	96.45	97.06
5.5	0.28	0.84	93.34	95.93	97.32	98.18
6.0	0.34	0.87	94.00	98.53	98.88	98.89
6.5	0.42	1.00	96.47	97.92	99.22	99.22
7.0	0.45	0.98	94.90	96.97	98.70	98.88
7.5	0.43	0.83	93.64	97.15	98.70	98.88
8.0	0.35	0.65	97.30	99.15	99.31	99.48
8.5	0.21	0.53	98.20	99.48	99.83	100
9.0	0.10	0.45	98.80	100	100	100

Table 2. Error statistics of v at different height

Height (km)	Mean difference	Root mean square	Proportion on relative deviation			
			<5%	<10%	<15%	<20%
0.5	-0.42	0.53	76.96	78.34	80.59	83.53
1.0	-0.22	0.47	78.25	79.70	79.95	80.20
1.5	-0.05	0.55	62.98	81.83	89.53	93.08
2.0	0.03	0.67	81.66	89.62	92.65	94.46
2.5	0.13	0.77	88.67	92.30	94.03	95.67
3.0	0.27	0.80	92.47	94.29	95.42	96.19
3.5	0.49	0.93	93.94	95.16	95.67	96.28
4.0	0.67	1.05	94.38	94.98	95.33	95.93
4.5	0.10	0.70	82.79	90.66	92.73	94.12
5.0	-0.12	0.80	54.84	71.63	83.82	90.74
5.5	-0.23	0.91	52.91	58.30	67.65	75.69
6.0	-0.26	1.01	51.44	56.14	61.51	74.53
6.5	-0.27	1.10	51.66	65.85	66.96	79.00
7.0	-0.25	0.95	53.20	56.23	69.60	73.24
7.5	-0.18	0.73	58.56	60.21	71.51	72.80
8.0	-0.09	0.55	63.84	67.13	70.33	73.62
8.5	-0.00	0.50	54.07	59.95	65.50	70.95
9.0	0.05	0.50	53.03	63.80	72.43	81.92

Table 3. Error statistics of w at different height

Height (km)	Mean difference	Root mean square	Proportion on relative deviation			
			<5%	<10%	<15%	<20%
0.5	0.02	0.19	89.10	89.62	89.97	90.31
1.0	0.01	0.36	82.79	83.56	84.08	84.60
1.5	0.00	0.59	79.58	81.57	82.87	83.74
2.0	-0.01	0.83	76.64	78.37	81.14	83.56
2.5	-0.03	1.10	73.10	75.52	78.03	80.45
3.0	-0.04	1.34	73.01	74.48	76.47	78.55
3.5	-0.05	1.57	68.94	71.28	73.10	74.91
4.0	-0.07	1.72	66.44	68.25	70.07	71.54
4.5	0.09	1.86	64.27	66.00	67.91	69.55
5.0	-0.11	1.98	62.02	63.58	64.88	66.44
5.5	-0.14	1.93	58.65	60.64	62.54	63.49
6.0	-0.16	1.60	68.36	68.96	70.80	71.87
6.5	-0.18	1.40	62.47	63.90	64.51	74.81
7.0	-0.19	1.39	60.57	61.44	61.90	73.37
7.5	-0.20	1.41	60.57	61.39	62.23	72.99
8.0	-0.21	1.51	62.39	62.73	63.64	63.94
8.5	-0.22	1.64	56.06	56.23	56.83	57.87
9.0	-0.24	1.82	64.45	64.53	64.71	66.88

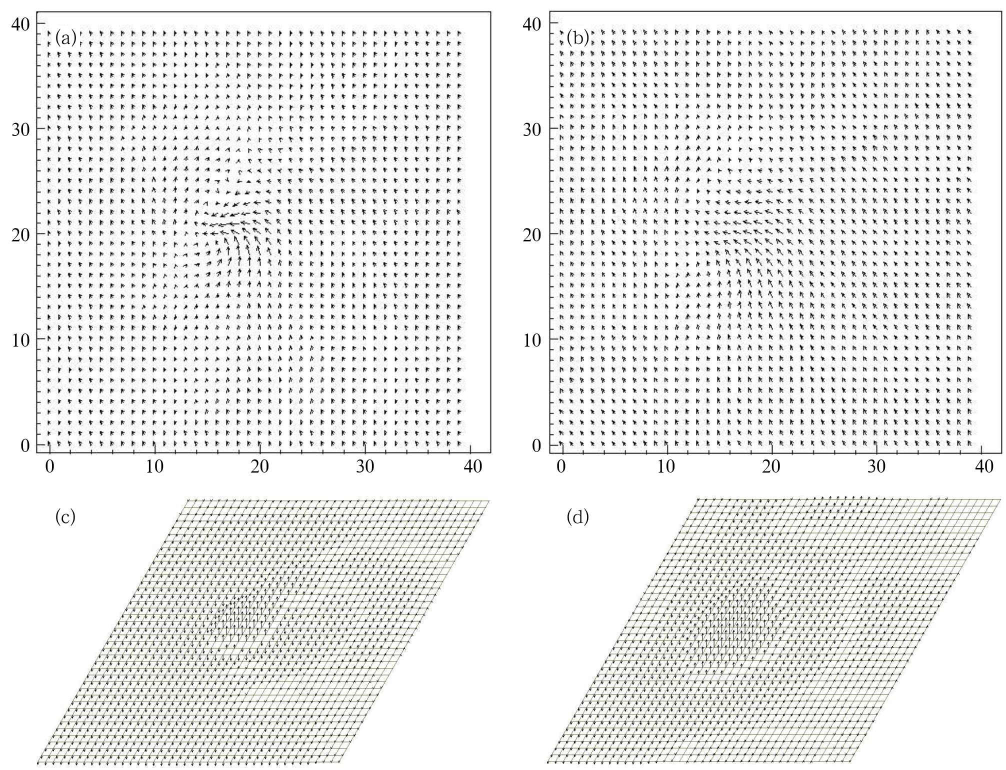

Fig.3. Horizontal velocity and vertical velocity at z=3 km. (a) Simulated horizontal velocity, (b) retrieved horizontal velocity, (c) simulated vertical velocity, and (d) retrieved vertical velocity.

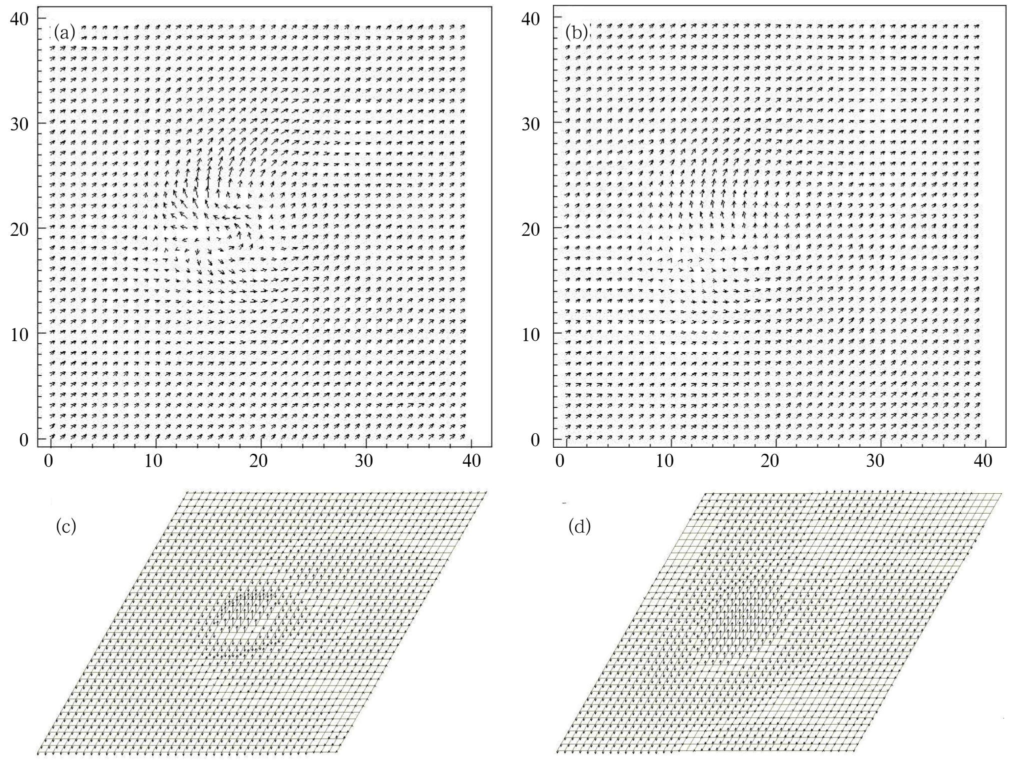

Fig.4. As in Fig.3 except for the height of 5 km.

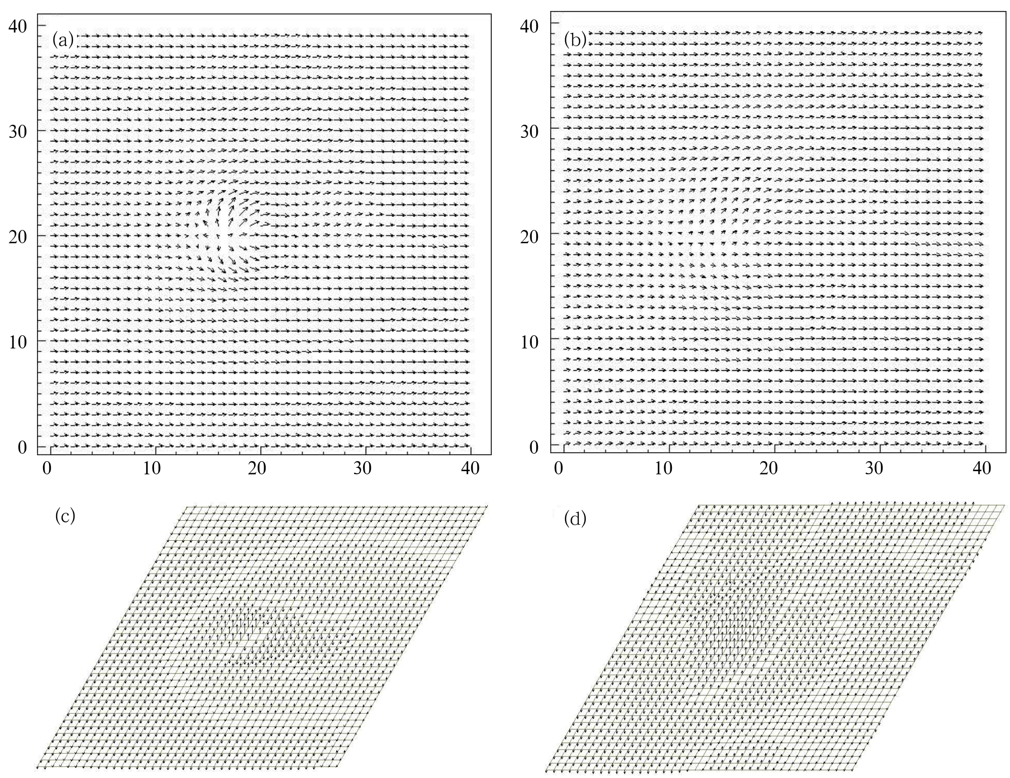

Fig.5. As in Fig.3 except for the height of 7 km.

From Fig.4, it is apparent that the retrieved horizontal wind is uniform with simulated one at 5 km level. The position of the retrieved storm center is quite similar to the simulated one. The pattern of the retrieved vertical velocity is much the same as the simulated one.

Figure 5 compares the retrieved wind and simulated one at z=7 km. It is similar in many respects to the result at low levels.

The result shown by these figures is consistent with the error statistics. The retrieved wind at the low and middle levels is more accurate than that at high levels due to the error accumulation in the integration of mass continuity equation. Furthermore, the radar observed point is not consistent with the numerical model grid point. The 3D velocity fields at the radar observed points are deduced by using Cressman interpolation method, and this is also one of the causes for retrieval errors.

On the whole, the comparative study shows that the retrieved wind at 8 km level is quite similar to the simulated one. The mesoscale weather system is often confined below 10 km. As a result, we can draw a conclusion that this retrieved technology can be used to retrieve the real 3D wind.

4. Conclusion

The notable advantage of the technology is that the three-dimensional wind field were solved simultaneously because the variational method was used. It also reduces the retrieved error and removes the ill-condition problem of the retrieval equations in the iterative method. The conventional COPLAN method and other variational retrieval method based on COPLAN method include two interpolation steps: interpolation from a spherical coordinate to a COPLAN coordinate system, and interpolation from a COPLAN coordinate system to a Cartesian coordinate system after the retrieval is completed. Significant errors can be introduced in the interpolation processes. This paper combines Cressman interpolation into one step in the variational function. This interpolation technology can preserve the radial nature of radar observations and improve the retrieval accuracy.

Eliminating the error accumulation in integrating mass continuity equation is one of the difficulties to overcome in the retrieval technology. In this paper, error accumulation in the integration of continuity equation has been reduced by applying the least squares adjustment of continuity equation as a constraint which improves the velocity estimates at high levels.

This paper studied the 3D wind retrieval technology using simulated dual-Doppler radar data. The experiment shows that the retrieved results have an acceptable precision for altitudes up to 8 km. Generally speaking, the mesoscale weather system is confined below 10 km. This method has the potential for retrieving the 3D wind and can be used in operation and in research.

We plan to do further study on this method, because the processing method of real radar raw data is more complex compared with simulated radar data.

Acknowledgements. We would like to thank Professor Xu Huanbin for his help and his three-dimensional cloud numerical model.

REFERENCES

Armijo, L., 1969: A theory for the determination of wind and precipitation velocities with Doppler radar. *J. Atmos. Sci.*, **26**, 570-573.

Bousquet, O., and M. A. Chong, 1998: Multiple-Doppler synthesis and continuity adjustment technique (MUSCAT) to recover wind components from Doppler radar measurement. *J. Atmos. Oceanic Tech.*, **13**, 343-359.

Chong, M., and C. Campos, 1996: Extended overdetermined dual-Doppler formalism in synthesizing airborne Doppler radar data. *J. Atmos. Oceanic Tech.*, **13**, 581-597.

Cressman, G. W., 1959: An operational objective analysis system. *Mon. Wea. Rev.*, **87**, 367-374.

Doviak, R. J., and S. Z. Dusan, 1984: *Doppler Radar and Weather Observation*. Academic Press, 458pp.

Lhermitte, R. M., and L. J. Miller, 1970: Doppler radar methodology for the observation of convective storms. 14th Radar Meteorology Conference, *Amer. Meteor. Soc.*, 133-138.

Miller, L. J., and R. G. Strauch, 1974: A dual-Doppler radar method for the determination of wind velocities within precipitating weather systems. *Remote*

Sens. Environ, **3**, 219-235.

Ray, P. S., C. L. Ziegler, W. Bumgarner, et al., 1980: Single and multiple Doppler radar observations of tornadic storms. *Mon. Wea. Rev.*, **108**, 1607-1625.

Xu Huanbin and Wei Shaoyuan, 1995: The modeling study of downburst. *Acta Meteorologica Sinica*, **53**, 168-175. (in Chinese)

Zhang Peiyuan, He Ping, Song Chunmei, et al., 1998: A study on error distribution and radar optimum arrangements of wind field measurement with Doppler radars. *Acta Meteorologica Sinica*, **56**, 96-103. (in Chinese)

Zhang Peiyuan, Zhou Haiguang, and Hu Shaoping, 2002: Reliability study for the determination of wind with dual-Doppler radars. *J. App. Meteor. Sci.*, **13**, 485-496. (in Chinese)